

Effective and Efficient Photo -Based PM2.5 Concentration Estimation

Guanghui Yue¹, Ke Gu¹, and Junfei Qiao, *Member, IEEE*

Abstract—Air pollution has become a worldwide concerned issue and automatical estimation of air quality can provide a positive guidance to both individual and industrial behaviors. Given that the traditional instrument-based method requires high economic, labor costs on instrument purchase and maintenance, this paper proposes an effective, efficient, and cheap photo-based method for the air quality estimation in the case of particulate matter (PM2.5). The success of the proposed method lies in extracting two categories of features (including the gradient similarity and distribution shape of pixel values in the saturation map) by observing the photo appearances captured under different PM2.5 concentrations. Specifically, the gradient similarity is extracted to measure the structural information loss with the consideration that PM2.5 attenuates the light rays emitted from the objects and accordingly distorts the structures of the formed photo. Meanwhile, the saturation map is fit by the Weibull distribution to quantify the color information loss. By combining two features, a primary PM2.5 concentration estimator is obtained. Next, a nonlinear function is adopted to map the primary one to the real PM2.5 concentration. Sufficient experiments on real data captured by professional PM2.5 instrument demonstrate the effectiveness and efficiency of the proposed method. Specifically, it is highly consistent with real sensor's measures and requires low implementation time.

Index Terms—Air quality estimation, gradient similarity, photo-based, PM2.5 concentration, saturation map.

I. INTRODUCTION

IN THE past decades, frustrating environmental change has appeared due to the excessive pursuit of rapid economic development as well as forward urbanization and industrialization. Among those environmental problems, air

Manuscript received June 15, 2018; revised November 13, 2018; accepted November 16, 2018. This work was supported in part by the National Science Foundation of China under Grant 61703009, in part by the Beijing Advanced Innovation Center for Future Internet Technology under Grant 110000546619001, in part by the Young Elite Scientist Sponsorship Program by the China Association for Science and Technology under Grant 2017QNRC001, and in part by the Nova Programme Interdisciplinary Cooperation Project under Grant Z161100004916041. The Associate Editor coordinating the review process was Huang-Chen Lee. (*Corresponding author: Ke Gu.*)

G. Yue is with the Beijing Advanced Innovation Center for Future Internet Technology, Beijing Key Laboratory of Computational Intelligence and Intelligent System, Faculty of Information Technology, Beijing University of Technology, Beijing 100124, China, and also with the School of Electrical and Information Engineering, Tianjin University, Tianjin 300072, China (e-mail: guanghuiyue.doctor@gmail.com).

K. Gu and J. Qiao are with the Beijing Advanced Innovation Center for Future Internet Technology, Beijing Key Laboratory of Computational Intelligence and Intelligent System, Faculty of Information Technology, Beijing University of Technology, Beijing 100124, China (e-mail: guke.doctor@gmail.com; junfeiq@bjut.edu.cn).

Color versions of one or more of the figures in this paper are available online at <http://ieeexplore.ieee.org>.

Digital Object Identifier 10.1109/TIM.2018.2886091



Fig. 1. Examples of various PM2.5 detection and measurement equipment.

pollution, known as one of the most relevant factors that endanger people's health, has been greatly aroused the crisis awareness [1]–[3]. Nowadays, the air quality index monitored individually or officially is almost the necessity before residents going out in major cities in China [4], [5].

Broadly, the air pollutants can be divided into the gaseous pollutant and aerosol pollutant. Typical gaseous pollutants includes the sulfur dioxide, nitrogen oxide, and carbon monoxide [6], [7]. According to the differences of physical properties, the aerosol pollutant can be classified into dust, fume, fly ash, smoke, fog, etc [8]. It is worth noting that the fine particulate matter (PM2.5) with the aerodynamic diameters of $2.5 \mu\text{m}$ or less can be suspended in the air for a long period of time and is easy to intrude into the lungs, thereby threatening the health by transmitting virus and hazardous chemicals into the human bodies. To monitor or measure the degree of PM2.5 concentration, many electronic instruments and sensors are designed and applied into the daily life. Some examples are shown in Fig. 1. The success of this equipment rests with the reasonable usage of physicochemical properties of PM2.5 [9]. Clearly, a high-precision instrument or sensor provides more precise results than a general one. However, it inevitably requires high economic costs on instrument purchase and setup as well as massive labor costs on instrument maintenance, thereby limiting the application range of these equipment. It is meaningful to design more handy solutions for resident reference [10], [11].

In the literature, the cooperation of electronic imaging equipment and computer platforms provides us a new thought that we can monitor and gauge physical events (e.g., medical diagnosis [12], quality evaluation [13]–[17], target detection [18], [19], and content edit [20]) in a relatively affordable and precise way [21]. Nowadays, smartphones are with high-quality imaging ability and high operating speed and gradually become one of the most needful elements in

daily life. With a smartphone, one can describe and record the scenes around us anytime and share the image with others easily. To some extent, the above facts naturally motivate the generation of ideas that the air quality in the case of PM2.5 concentration can be estimated by analyzing the characteristics of captured images. Although the idea is very attractive, it is not an easy task but full of challenges and difficulties. To date, only very few attempts have devoted in this way. For example, Wang *et al.* [22] proposed a pioneering work to estimate the PM2.5 concentration by computing the coefficient of light extinction from the color image. In [23], the transmission matrix was first estimated and, in parallel, the depth map was calculated via deep convolutional neural fields. Then, the PM2.5 concentration was computed by incorporating these two parts. Liu *et al.* [24] attempted to estimate the PM2.5 concentration by extracting six image features. Specifically, the image transmission feature was first extracted according to the dark channel prior. Then, the contrast and entropy were captured to reflect the image clarity. Next, the solar zenith angle was estimated. In addition, the sky color and region were analyzed to consider the weather influence. Finally, all these features were pooled together via a regression function learned by support vector regressor to infer the PM2.5 concentration. Pan *et al.* [25] proposed a two-stage air quality prediction scheme. First, the haziness of an image was estimated. Then, the haziness map was feeded into a convolutional neural network to estimate the air quality. In [26], an air quality estimation model was built by operating on statistics computed from the pixel color values of the sky regions, which were automatically detected via deep learning.

According to the discussions above, it is clear that the photo-based PM2.5 concentration estimation is still in its infancy and some limitations exist. On the one hand, some methods based on handcraft features require the weather, sky region, or depth information beforehand, which hinders the automatical ability and, thus, largely limits their application scopes. On the other hand, all these learning-based methods highly rely on the training data set, which indicates that the sample distribution and size of the data set may play a direct role in the performance of the learned model. In practical applications, an automatical, effective, and efficient method is more in demand.

In this paper, we propose a novel photo-based PM2.5 concentration estimation method. Experimental results on real captured data demonstrate its effectiveness and efficiency. The proposed method presents three major contributions. First, compared with aforementioned photo-based methods, the proposed one is completely blind, indicating that it is able to be implemented anytime without pretrain procedure beforehand. Meanwhile, it does not rely on any additional auxiliary information (e.g., depth information and camera position) but addresses the PM2.5 concentration estimation problem via simple analysis of image characteristics. Second, through comparisons, we find that the saturation channel has different appearances between images captured under different PM2.5 concentrations. The proposed method grasps this observation and estimates the PM2.5 concentration by extracting the intensity distribution shape of saturation map

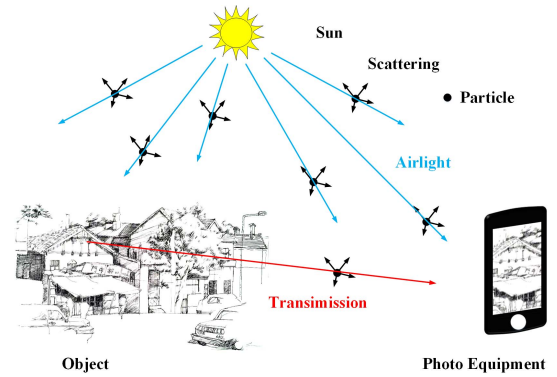


Fig. 2. Simple illustration of the reached radiance of the smartphone camera for imaging.

and calculating the gradient similarity between it and the gray-scale map. Specifically, the PM2.5 concentration is estimated by combining these two parts followed by a nonlinear mapping procedure. Third, the proposed method requires lower run time than competing methods.

The remainder of this paper is arranged as follows. Section II illustrates the characteristics of images captured under diverse PM2.5 concentrations and introduces the proposed method in detail. In Section III, extensive experiments are conducted to validate the effectiveness of the proposed method as well as make comparisons with the state-of-the-art relevant estimation methods. Besides, some discussions and analyses are also presented in Section III. Finally, the conclusion is given in Section IV.

II. OBSERVATIONS AND THE PROPOSED METHOD

In this section, we first present several observations regarding images captured under different PM2.5 concentrations, based on which, we then propose a novel PM2.5 concentration estimation method. More details are given in the following.

A. Observations

The successful and broad usage of electronic cameras fundamentally benefits from subtly utilizing the principle of small hole imaging. Generally, the imaging procedure has two stages. First, the light rays of the object transmit through the lens. Then, the photosensitive materials (e.g., the film and complementary metal–oxide–semiconductor) inside the camera capture the rays and accordingly form the image by chemical or photoelectric reaction. Clearly, the light rays determine the type and content of the formed image. In real scenes, the captured image consists of multiple objects, such as buildings, animals, plants, sky, and water. The light rays emitted from them are transmitted into the lens through the air. Ideally, the formed image can well record the real appearance of those objects with the hypothesis that the air has no impact on the light rays' transmission. However, such a hypothesis is no longer established in the case of particle pollution. To illustrate this, one simple schematic is given in Fig. 2, where the black dot denotes the particle. For the sake of discrimination, the airlight, light emitted by objects, and light scattered by particles are depicted in blue, red, and

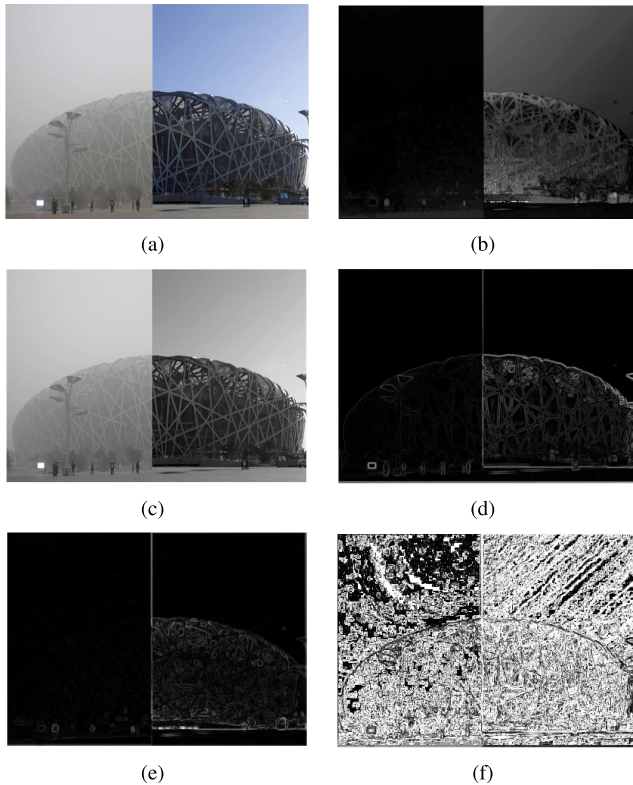


Fig. 3. Comparisons between photographs captured under high and low PM_{2.5} concentrations. (a) Mixed sample photograph, and (b) and (c) its saturation and gray-scale maps, respectively. (d) and (e) Gradient maps of (c) and (b), respectively. (f) Gradient similarity map between (b) and (c).

black, respectively. In the case of pollution, the air is suffused with a number of suspended particles, which attenuate the light transmission greatly. The attenuation of light transmission via scattering can be expressed by the Beer–Lambert law, which indicates that the particle size and concentration have a direct impact on the attenuation degree. Specifically, these suspended particles interact with light rays in the form of scattering, including Rayleigh scattering and Mie scattering [27]. If the size of particles is much smaller than the wavelength of the light ray, Rayleigh scattering dominates and is responsible for the blue color of the sky. Conversely, the Mie scattering occurs and tends to produce a white glare around the sun when the size of particles is comparable to the wavelength of the light ray. As a result, the appearance (e.g., structure, brightness, and color saturation) of the captured image is greatly affected by the combination of the Rayleigh scattering and Mie scattering [24], [27]. Obviously, denser concentration of particles would cause a severe attenuation of light transmission and accordingly affect more on image characteristics.

Fig. 3(a)¹ provides an intuitive illustration of suspended particles' impact on the imaging effect. The left and right halves of the photograph are captured outdoors under different PM_{2.5} concentrations. Specifically, the left half has a high PM_{2.5} concentration while the right half has a low PM_{2.5} concentration. Since it is almost symmetric, Fig. 3(a)

is one ideal choice for comparisons by avoiding the content impact. Clearly, the photograph captured in the high PM_{2.5} concentration loses some details (with low contrast) and colorfulness compared to that captured in the low PM_{2.5} concentration [28], [29]. Moreover, we also decompose the color image into hue, saturation, and value maps. Much to our excitement, these three maps exhibit entirely different appearances in the case of diverse air quality conditions. Among them, the one attracting our attention most is the saturation map, as shown in Fig. 3(b). By observing Fig. 3(b) carefully, one can find that the saturation map is lack of structural information, and its pixel values tend to be 0 under a high PM_{2.5} concentration. In contrast, the saturation map preserves main structures, and its pixel values disperse throughout the intensity range in the case of a low PM_{2.5} concentration. Overall, the PM_{2.5} concentration affects the imaging effect, and a higher concentration produces severe impacts on the image appearance. Actually, the difference between the left and right halves of Fig. 3(a) is the result of the combination of multiple suspended particles' impacts on the light scattering. In this paper, we simply assume that the PM_{2.5} concentration is a good indicator for reflecting the total suspended particles, and a high concentration denotes a high total suspended particle degree. In this sense, the characteristics (e.g., structure and color saturation) of the captured photograph can be used to estimate the PM_{2.5} concentration.

B. Proposed PM_{2.5} Concentration Estimation Method

According to the aforementioned observations, we propose a novel photograph-based PM_{2.5} concentration estimation method in this section. Specifically, the proposed method aims to tackle this estimation problem in two aspects.

How to measure the structural information loss is the first considered aspect. One simple and direct way is calculating the gradient map, which has been broadly used in image processing for reflecting structures [30]–[32]. However, images are with diverse contents and structures, directly applying the gradient information for PM_{2.5} concentration estimation may cause the performance bias. Fortunately, studies on image quality assessment state that calculating the structural similarity between one high-quality image and its corrupted version can effectively avoid the content's impact [33]–[35]. Although attractive, it is hard to obtain the associated clean image without influence from particles when capturing an image in the case of particle pollution. Here, we propose an alternative way to quantify the structural similarity and use it to measure structural information loss.

Fig. 3(c) shows the gray-scale map of Fig. 3(a). It is obvious that the main structures of objects (such as the building and characters' silhouette) are preserved under both high and low PM_{2.5} concentrations. By contrast, the appearances of saturation maps under two conditions are at opposite poles, as shown in Fig. 3(b). Clearly, the one in the case of the high concentration almost loses all the structural information, while the one under the low concentration still contains the main structures. The comparison results between Fig. 3(b) and (c) inspire us to quantify the structural information loss by

¹The photograph is downloaded from Internet and the copyright belongs to its rightful owners. No copyright infringement is intended.

computing the gradient similarity between them. Specifically, given an RGB-format color image I , we first converted it into the gray-scale format J

$$J(x, y) = \mathbf{rgb2gray}(I(x, y)) \quad (1)$$

where $\mathbf{rgb2gray}(\cdot)$ is the operator to transform color image into gray-scale map. x and y are pixel indices in horizontal and vertical directions, respectively. Then, we decompose I to obtain the saturation map S

$$S(x, y) = \begin{cases} \frac{M(x, y) - N(x, y)}{M(x, y)}, & \text{if } M(x, y) \neq 0 \\ 0, & \text{otherwise} \end{cases} \quad (2)$$

where $M(x, y) = \mathbf{max}[R(x, y), G(x, y), B(x, y)]$ is the maximum value calculated by the maximum operator $\mathbf{max}[\cdot]$ among three color channels (i.e., R, G, and B). Likewise, $N(x, y) = \mathbf{min}[R(x, y), G(x, y), B(x, y)]$ is the minimum value computed by the minimum operator $\mathbf{min}[\cdot]$. Next, the gradient map of the gray-scale and saturation maps are computed as follows²:

$$\begin{cases} G_J(x, y) = [(J(x, y) \otimes p_x)^2 + (J(x, y) \otimes p_y)^2]^{\frac{1}{2}} \\ G_S(x, y) = [(S(x, y) \otimes p_x)^2 + (S(x, y) \otimes p_y)^2]^{\frac{1}{2}} \end{cases} \quad (3)$$

where \otimes is the convolution operator. p_x and p_y are filter kernels in horizontal and vertical directions, respectively. In this paper, we adopt the Prewitt filters due to their simplicity. Formally, they are defined as follows:

$$p_x = \begin{bmatrix} 1/3 & 0 & -1/3 \\ 1/3 & 0 & -1/3 \\ 1/3 & 0 & -1/3 \end{bmatrix}, \quad p_y = p_x^T \quad (4)$$

where T denotes the transpose operation. Fig. 3(d)–(e) depicts the obtained gradient maps. As seen, the gradient map [Fig. 3(d)] obtained from the gray-scale map can well portray main structures of photographs captured in both PM2.5 concentrations. In contrast, the gradient map [Fig. 3(e)] obtained from the saturation map exhibits different appearances. Specifically, the left half of Fig. 3(e) presents flat appearance, while the right one preserves main structures. This directly illustrates the particles' impact on structural corruption. To better distinguish the difference between two gradient maps, the readers are advised to enlarge the figures during viewing.

After obtaining the gradient maps, we calculate their similarity map K

$$K(x, y) = \frac{2G_J(x, y) \cdot G_S(x, y) + C_1}{G_J^2(x, y) + G_S^2(x, y) + C_1} \quad (5)$$

where $C_1 = 0.01$, and it is a constant to avoid zero denominator. A larger K value indicates the higher structural information preservation, and vice versa. Fig. 3(f) shows the similarity map (ranging from 0 to 1) between Fig. 3(d) and (e). Clearly, the similarity map (especially the sky region) exhibits different appearances under two PM2.5 concentrations. Given that natural images consist of multiple local regions with diverse contents, and these regions suffer from different structural

²It is worth noting that the saturation map should be mapped into range [0 255] before the gradient map calculation.

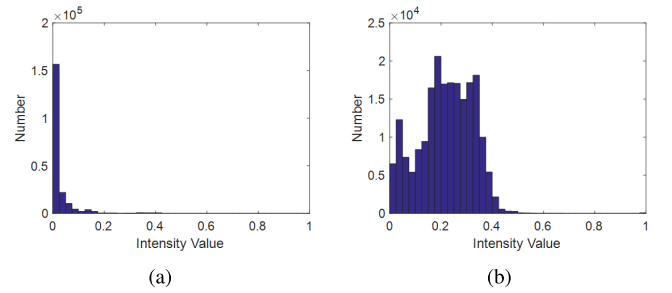


Fig. 4. Pixel values distributions of the left and right halves of Fig. 3(b).

degradations, we propose to calculate the standard deviation Q_s of the gradient similarity map to quantify the structural information loss

$$Q_s = \sqrt{\frac{1}{H} \sum_{h=1}^H (K_h - \bar{K})^2} \quad (6)$$

with the mean value defined by

$$\bar{K} = \frac{1}{H} \sum_{h=1}^H K_h \quad (7)$$

where K_h is the h th value in K . H is the total pixel number in the gradient similarity map. The larger the Q_s value is, the more structural the information loses are, and thus, the severer the PM2.5 concentration happens.

Saturation refers to the degree of color vividness. By analyzing saturation, we are able to know the purity of image color. As stated above, the particles corrupt the light rays emitted from the scenes; therefore, the formed image is colorless with small saturation values. Also taking the saturation map as the breakthrough, our second consideration is how to quantify its flat appearance from the statistical way. Fig. 4 separately shows the distribution maps of left and right halves of Fig. 3(b). It is obvious that the distributions obtained under high and low PM2.5 concentrations exhibit different distribution shapes. To be specific, most pixel values in Fig. 4(a) tend to be 0, and the associated pixel number decreases with the value increases. By contrast, those in Fig. 4(b) exhibit unimodal, first increasing and then decreasing. Therefore, effectively capturing such distribution characteristics may benefit to estimate the degree of PM2.5 concentration. According to observation, we simply assume that the pixel values in saturation map could be coarsely fit by the Weibull distribution. Formally, the probability density function of the Weibull distribution can be expressed as follows:

$$f(s, \alpha, \beta) = \frac{\beta}{\alpha} \left(\frac{s}{\alpha}\right)^{\beta-1} \cdot e^{-\left(\frac{s}{\alpha}\right)^\beta} \quad (8)$$

where s is the response of saturation map S . α and β are two parameters to control the shape and scale of the distribution. Fig. 5 presents the curves under different parameter settings. The red, black, and magenta curves are the plots of (8) under the conditions $\alpha = 1, 3, \text{ and } 5$ with fixed $\beta = 0.5$. Clearly, α determines the slope degree of the distribution. Likewise, the red, green, and blue curves are the plots under

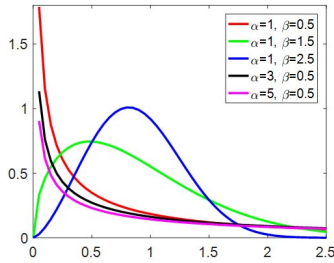


Fig. 5. Illustration of the impacts of α and β on the Weibull distribution.

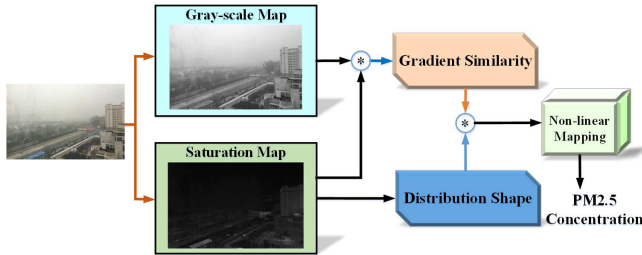


Fig. 6. Framework of the proposed PM_{2.5} concentration estimation method.

the conditions $\beta = 0.5, 1.5, \text{ and } 2.5$ with fixed $\alpha = 1$, which means that β controls the scale attribute. Given the data distribution, these two parameters can be computed via the maximum likelihood estimation [36]. Since the pixel values of the saturation map tend to be 0 in the case of high PM_{2.5} concentration, we only adopt α to quantify the delay degree of saturation values in this paper. As α is extracted on the saturation distribution, it, to a certain extent, reflects the color information. Here, we take it as another feature (denoted as Q_w) to estimate the degree of the PM_{2.5} concentration from the viewpoint of measuring color information.

Based on the aforementioned discussions, we have obtained two features. Here, we combine them to infer the primary PM_{2.5} concentration Q

$$Q = Q_S^\nu \cdot Q_w^{1-\nu} \quad (9)$$

where ν is the parameter to judge the relative significance of the two components. It requires to state that Q is not the actual value that accurately quantifies the PM_{2.5} concentration but the relative value. That is to say, Q can judge the relative PM_{2.5} concentration among a group of photographs. To estimate the actual PM_{2.5} concentration, it requires a nonlinear mapping procedure, which can help to improve the performance accuracy but maintain the monotonicity of input data. In this paper, the five-parameter logistic function is adopted

$$P(Q) = \tau_1 \cdot \left[\frac{1}{2} - \frac{1}{1 + e^{(Q-\tau_2)/\tau_3}} \right] + \tau_4 \cdot Q + \tau_5 \quad (10)$$

where $P(Q)$ is the mapped score set that can estimate the PM_{2.5} concentration with the same range as that of the instrument-based method. Parameters $\{\tau_1, \tau_2, \dots, \tau_5\}$ are ascertained during the curve fitting procedure. For convenience, Fig. 6 gives the basic framework of the proposed method. For the captured photograph, it is first converted into

gray-scale and saturation maps, based on which the gradient similarity is then computed. Next, the distribution shape of the saturation map is estimated using the Weibull distribution. Finally, the standard deviation of the gradient similarity map and the distribution shape parameter are combined to give the primary PM_{2.5} concentration Q . The final PM_{2.5} concentration (in the unit of $\mu\text{g}/\text{m}^3$) is estimated by feeding Q into the nonlinear mapping function [i.e., (10)].

III. EXPERIMENTAL RESULTS

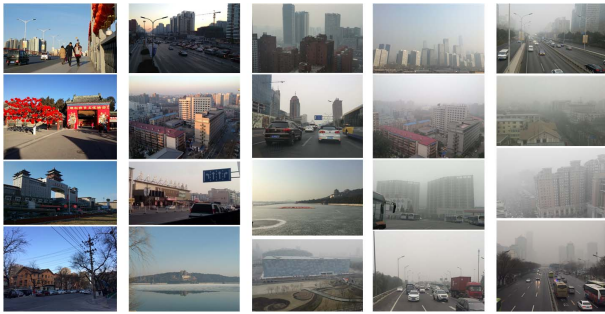
A. Experiment Protocol

1) *Testing Data Set*: The air quality image database (AQID) used in [37] is selected as the test platform for the validation and comparison. Specifically, AQID contains 750 photographs captured by cameras under different PM_{2.5} concentrations in the past three years. Multiple scenes, including square, temple, flyover, lakes, roads, cars, parks, and buildings, are involved so that they can approximately characterize the distributions of air quality in natural scenes. The resolutions of these photographs range from 500×261 to 978×550 . The associated PM_{2.5} value of each photograph is given through the retrieve from the historical data of hourly PM_{2.5} concentration values provided by the U.S. embassy in Beijing. These accurate values are detected by the instrument MetOne BAM-1020, which uses the β -ray absorption method. During image acquisition, two basic rules are obeyed to guarantee the sample quality. The first rule is that the image should be captured on a clear day without the wind or with the slight wind, and the captured place should be within a 1-km radius of an air quality monitoring site. By restricting the wind and place, it can, to the largest extent, ensure that the retrieved PM_{2.5} value associated with the captured image is approximate to the real PM_{2.5} value reported by the monitoring site. The second rule is that the captured image must contain sky, which approximately occupies the top 1/3–1/2 area of the image, and avoid to facing the sun. This is used to avoid the image captured indoor and based on the consideration that the sky region is sensitive to the PM_{2.5} concentration. For the whole data set, the PM_{2.5} concentration values range from 1 to $423 \mu\text{g}/\text{m}^3$. (A lower value indicates the better air quality.) Fig. 7 presents some examples and plots the histogram of the PM_{2.5} values in AQID.

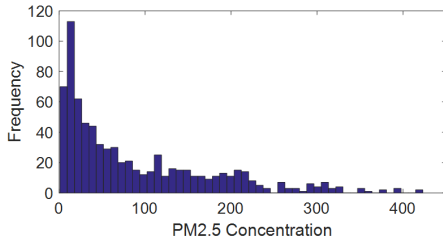
2) *Evaluation Criteria*: The performance can be evaluated and compared among different objective methods from two aspects, i.e., the prediction error and monotonicity. In this paper, we adopt the root-mean-square error (RMSE) to measure the prediction error. By definition, the RMSE can be expressed as follows:

$$\Lambda_R = \sqrt{\frac{1}{Z} \sum_{z=1}^Z (\gamma_z - A_z)^2} \quad (11)$$

where $Z = 750$, and it is the number of images in the test data set, γ_z is the estimated score of the z th photograph by an objective method. For the proposed method, $P(Q_z) = \gamma_z$. Likewise, A_z is the real PM_{2.5} value associated with the z th photograph.



(a)



(b)

Fig. 7. (a) Examples of the testing data set. From the first to the last columns, the PM2.5 values are within [0 50], [51 100], [101 200], [201 300], and [301 423] (the unit is $\mu\text{g}/\text{m}^3$), respectively. (b) Histograms of PM2.5 concentration values in AQID.

We also utilize the Spearman rank-order correlation coefficient (SRCC) and the Kendall's rank-order correlation coefficient (KRCC) for validating the prediction monotonicity. The SRCC is formally calculated by

$$\Lambda_S = 1 - \frac{6 \sum_{z=1}^Z d_z^2}{Z(Z^2 - 1)} \times 100\% \quad (12)$$

where d_z is the difference between the z th values ranks in γ and A . KRCC can be computed as

$$\Lambda_K = \frac{2(Z_c - Z_d)}{Z^2 - Z} \times 100\% \quad (13)$$

where Z_c and Z_d are the numbers of concordant and discordant pairs across the data set. It is worth noting that an effective method should obtain high values in Λ_S and Λ_K (with the maximum value is 100%) and a small value in Λ_R (with the ideal value is 0).

3) *Parameter Settings*: In the proposed method, only one parameter ν in (9) should be determined before comprehensive experiments. Actually, ν controls the relative significance between the two parts, i.e., Q_S and Q_w . To gauge its suitable value, we set it from -1.001 to 1 in an interval of 0.05 and report the associated KRCC, SRCC, and RMSE values in Fig. 8. Through observation, we find that the KRCC, SRCC, and RMSE values tend to be gentle with good results when ν ranges from -1 to 0.2 , and change greatly when ν ranges from 0.2 to 1 . Therefore, we set ν as -0.56 to simultaneously obtain good KRCC, SRCC, and RMSE results. Besides, according to the descriptions in Section II-B, one may find that Q_S and Q_w are not sensitive to image size. Hence, the image size is downsampled by 8 for reducing the implementation time.

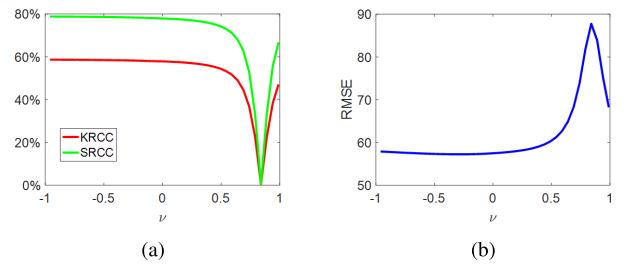


Fig. 8. Performance varies with different ν values. (a) KRCC and SRCC and (b) RMSE.

TABLE I
NUMERICAL COMPARISON RESULTS AMONG DIFFERENT METHODS.
THE TOP TWO RESULTS OF EACH CRITERION ARE
HIGHLIGHTED IN BOLD FACE

Methods	Λ_S	Λ_K	Λ_R	Rank	Run Time (s)
NIQE [38]	1.02%	0.58%	87.82	12	0.1243
IL-NIQE [39]	25.54%	17.26%	83.11	7	5.0507
LPSI [40]	1.81%	1.19%	87.78	11	0.0239
NIQMC [41]	44.34%	29.66%	79.87	4	2.1772
FISH [42]	40.36%	27.23%	77.91	6	0.0218
BIBLE [43]	3.41%	2.31%	87.83	10	1.7362
JNB [44]	14.25%	9.43%	86.34	8	0.1568
CPBD [45]	6.62%	4.36%	87.52	9	0.0943
MLV [46]	42.18%	28.70%	77.54	5	0.0505
BIQME [47]	53.75%	37.19%	73.78	3	1.0956
PPPC [37]	81.91%	60.81%	51.88	1	0.0515
Proposed	78.23%	58.09%	57.69	2	0.0164

B. Performance Comparisons

Given that the proposed method is proposed by analyzing image characteristics, in this paper, 11 methods designed for measuring image variations are selected as competing objects to fully validate the effectiveness and superiority of the proposed method. Based on the application scenarios, they can be broadly divided into three categories. The first category contains three lately designed methods for characterizing image naturalness, such as NIQE [38], IL-NIQE [39], and LPSI [40]. The second category involves recently proposed state-of-the-art methods for measuring image contrast and blurriness/sharpness, including NIQMC [41], FISH [42], BIBLE [43], JNB [44], CPBD [45], MLV [46], and BIQME [47]. The third category contains one recently proposed PM2.5 concentration prediction method, PPPC [37]. (Since we fail to obtain the source codes of works [22]–[24] and it is hard to recode them according to the limited description in the associated papers, no comparison is conducted with them.) The reason behind these selections lies in that particles attenuate the light rays via scattering, and the scattered part is captured by the electronic camera. As a result, the formed photograph has poor appearance compared with the original scene, such as low contrast, lacking naturalness, and losing structures. Among the aforementioned three categories, the first one performs well on measuring image naturalness. The second category is competent for gauging high-frequency components, which are able to reflect the contrast and structural information.

Table I tabulates the experimental results on the AQID database. For convenient viewing, the top two results in each criterion are highlighted in boldface, and the rank is

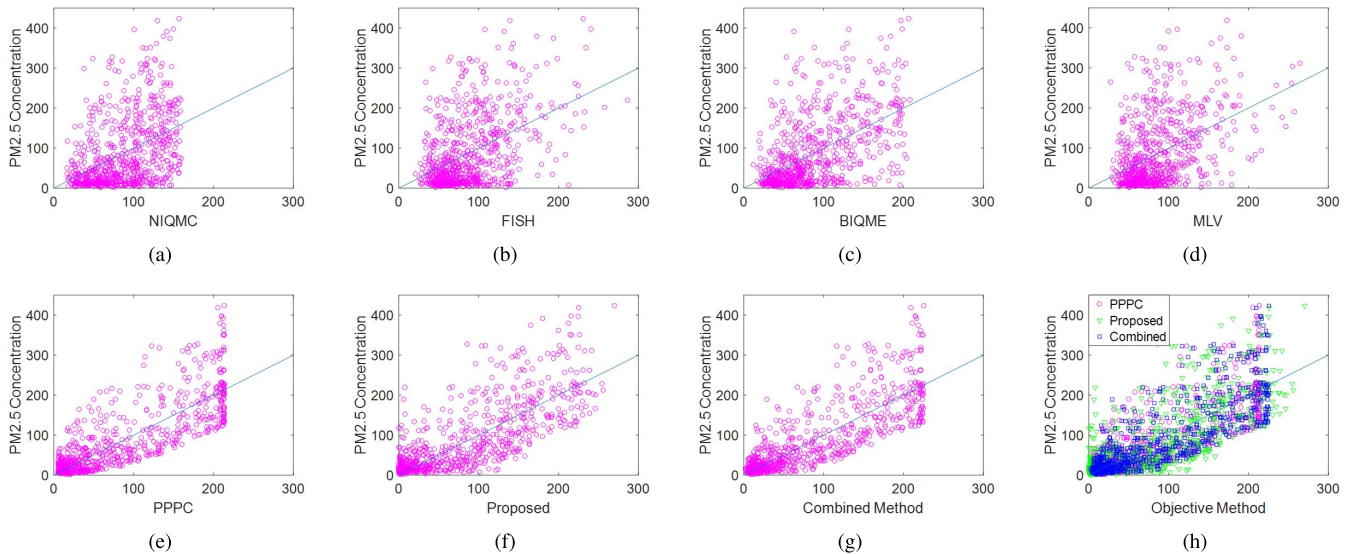


Fig. 9. Scatterplots. In each scatterplot, x-axis presents the estimated scores by an objective method and y-axis shows the associated PM_{2.5} concentrations. The blue line indicates the case of ideal prediction. For convenient comparison, we also present the scatterplots of PPPC, the proposed method, and the combined method in (h).

also given regarding the comparison among SRCC values. (Actually, the proposed method always ranks 2 no matter which evaluation criterion is used. Here, we just report the result in case of SRCC due to the limited space.) According to the data, we have the following observations. On the one hand, it is obvious and excited that the proposed method occupies the second place with good performance among all competing methods and is slightly inferior to PPPC (with approximately 3% performance drop on SRCC and KRCC values, respectively). The obtained SRCC and KRCC values are, respectively, over 78% and 58%, which leave a large room for improvement to the second runner-up (i.e., BIQME). More concretely, the proposed method has acquired approximately 25% SRCC gain and 21% KRCC gain compared to BIQME. On the other hand, the methods in the former two categories exhibit obviously different performance; therefore, none of the two categories has the full confidence to estimate the PM_{2.5} concentration effectively. Among them, the second category seems to be with slight superiority than the first category. However, it is far from securely utilizing these methods in that category for the PM_{2.5} concentration estimation due to the disappointing performance. In contrast, the PPPC and the proposed method obtain higher prediction monotonicity and lower prediction error; they are competent for solving the PM_{2.5} concentration estimation problem.

Reasonable explanations can be attributed to the follows. First, methods in the first category hold the hypothesis that the variations of pixel values may cause the change of natural images' specific regularity (denoted by the naturalness), and the degree of variations (caused by distortions such as blurriness, blockiness, and noise) has a direct relationship with that of regularity change [48]. Hence, these methods can effectively measure the distortion degree related to image naturalness. However, particles corrupt the light rays and accordingly induce different impacts on the image appearance

compared with traditional distortions, whether the appearance change relating to the regularity change is still unknown. Therefore, it is acceptable that these methods in the first category show their incapacity for PM_{2.5} concentration estimation. Second, these methods in the second category focus on measuring edge variation and contrast change, which are the main characteristics of blur and contrast distortions. In reality, the image captured in the high PM_{2.5} concentration not only contains edge variation but, in particular, loses edges, generates unordered faked small edges, and reduces color information, as shown in Fig. 3(a). As a result, simply measuring the sharpness or contrast on gray-scale map is insufficient. In contrast, PPPC and the proposed method address the concentration estimation problem by observing and measuring the difference between images captured under high and low PM_{2.5} concentrations. Specifically, PPPC builds a statistical model by analyzing quantifies of photographs captured under different PM_{2.5} concentrations. The proposed method tackles the estimation problem by extracting features to gauge color and structural information loss, which are sensitive to PM_{2.5} concentrations. Hence, both PPPC and the proposed method obtain promising performance.

Apart from the numerical results, we also provide the scatterplots to straightforwardly visualize the comparison, as shown in Fig. 9. Only the top five competing methods are selected by considering the prediction results tabulated in Table I. In each scatterplot, x-axis presents the estimated scores by an objective method and y-axis shows the associated PM_{2.5} concentrations. The blue line indicates the case of ideal prediction. It is clear that PPPC and the proposed method are superior to other competing methods with impressive monotonicity and convergency along the blue line. Specifically, the estimated scores of the proposed method range from 0 to 300, which is approximate to the range of real measured PM_{2.5} concentrations in the AQID (ranging from 0 to 423).

In contrast, some methods, e.g., PPC and NIQMC, have narrower range and are bounded by certain values. This may be attributed to that the extracted features in PPC and NIQMC have limited ability for quantifying severer distortions. As a result, for the image captured under a higher PM2.5 concentration, PPC and NIQMC lose their effectiveness. Apparently, it would be more accurate when the estimated scores and the ground truth have the same range. A larger range difference indicates larger prediction error. In this sense, the proposed method is more suitable for PM2.5 concentration estimation due to its broader response range.

As discussed above, PPC and the proposed method lead these competing methods. Here, we further investigate whether these two leading methods can be integrated to generate a more effective one. To this aim, we first combine the feature Q calculated by (9) and the extracted feature Q_P in PPC

$$U = Q^\tau \cdot Q_P^{1-\tau}. \quad (14)$$

Then, the U is feeded into (10) to estimate the PM2.5 concentration. Here, τ is set as -0.96 . Experimental results show that the combined method can obtain $\Lambda_S = 83.99\%$ and $\Lambda_K = 63.57\%$. By comparing the results in Table I, one can find that the combined method is superior to all methods and brings approximately 2% performance gains in SRCC and KRCC compared with PPC. Therefore, it is more suitable for the application focusing on effectiveness. For convenient viewing, we also present the scatterplot of the combined method in Fig. 9(g).

C. Run Time

In addition to effectiveness, efficiency is also an important factor for the comparison. A fast algorithm is more desired in practical applications. In this section, we investigate the run time of the proposed method and compare it with all competing methods. For fairness, all methods are implemented with the source code released by the associated authors on the same test environment (MATLAB2016b on a 64-bit desktop computer with Intel E5-1650 at 3.2-GHz CPU processor and 32-GB internal memory). The run time is recorded as the mean time required for the overall 750 photographs in the test data set. The last column of Table I gives the results. Obviously, the proposed method works very efficiently and is faster than all competing methods. Concretely, it only consumes 0.0164 s for processing a photograph and is almost three times faster than PPC. Given that most smartphones support for high-definition images and their processors are usually lower than the test desktop computer, more time is required to implement these algorithms in real applications. In view of this, our method has an advantage than competing ones.

D. Discussion

It is a new attempt to estimate the PM2.5 concentration by a photo-based method, with which, people can sufficiently exert the electronic camera and accessible network to monitor and share the concentration information anywhere and anytime. This paper proposes a novel method via analysis of

image characteristics. The success of the proposed method lies in that it estimates the color information on the saturation map and the structural information by computing the gradient similarity map between gray-scale and saturation maps. Extensive experiments have validated its effectiveness and efficiency. Specifically, the proposed method is slightly inferior to PPC but is more efficient than PPC. By combining it with PPC, we obtain a more effective one. Hence, we can select either it or the combined one in view of whether the application focuses more on effectiveness or efficiency. It is worth noting that, there are some limitations to the proposed method.

- 1) One critical hypothesis held in this paper is that the PM2.5 concentration is a good indicator for reflecting the total suspended particles, and a high concentration denotes a high total suspended particle degree. Actually, the particles are quite complex, and PM2.5 is just one of them. It is still unclear whether the PM2.5 concentration and total suspended particles have the monotonous relationship. Despite this, we can still obtain encouraging performance using this simple hypothesis, which indicates that we are in the right direction for addressing the problem in this paper. It might improve current performance if we know the accurate relationship. Another hypothesis is that the pixel values of the saturation map can be coarsely fit by the Weibull distribution according to observation. In fact, some images do not strictly obtain such hypothesis due to the content variations. Nevertheless, we can still obtain considerable results via the use of such coarse fitting, because it, to some extent, can quantify the distribution shape and accordingly estimate the PM2.5 concentration degree. To improve performance, more precise fitting is required in the future.
- 2) In addition to particles, the image characteristics can also be affected by other factors, such as the compression caused by the camera, the quality of the sensor in the camera, the angle of the camera to the sky, time of the day, season of the year, weather, and so on. Each factor has the individual impact on the characteristics. In this paper, we simply assume that the characteristics are merely affected by particles but without other factors. Therefore, the proposed method only estimates the PM2.5 concentration coarsely. To improve the accuracy, we must, to the largest extent, eliminate other elements' (except particles) impacts by obeying some rules during implementing the proposed method. First, it should avoid facing the sun when we capture a photograph. Naturally, a user can capture a sequence of photographs within 1 s, and choose anyone for the test on the premise of the selected one is normally exposed. The smartphone can be held by hand or stand without an obvious jitter. Second, the captured content should include the sky, and the sky region occupies the top 1/3–1/2 of the photograph. Third, we should avoid testing in sandstorms and foggy weather, because the fly ash and fog also have impacts on light scattering. The present method is incapable of distinguishing them. Fourth, a test should be conducted in the daytime. Sunlight is not available

but artificial light when capturing photographs at night. Since sunlight and artificial light have entirely different spectra, they may have different interactions with the particles. The current method may be not suitable for the night environment. Last, it encourages using a relatively high-quality camera to capture images, because a low-quality camera would cause more distortions on the image.

We do not expect that the proposed method will replace the professional PM_{2.5} measurement equipment, but use it to guide people to stay away from the suspected air pollution and promote the air pollution awareness. To keep this interesting topic going, we can conduct future work from the following aspects. First, more haze-sensitive features derived from the dark channel prior can be adopted and integrated into the proposed method for performance improvement [22]–[24], [49], [50]. For instance, we can simplify the imaging model under haze by utilizing the dark channel prior and derive the transmission matrix as a feature for PM_{2.5} concentration. Also, we may segment the photograph into sky and nonsky regions based on the dark channel prior. The proposed method can be further modified on different regions. Second, more refined features should be considered in estimating color and structural information. For example, a more precise fitting method is required for quantifying the distribution shape of saturation map. Third, how sensitive is the proposed method to the test environment, such as the light intensity, humidity, camera angle, camera quality, time of the day, and season of the year, remains an open issue. More careful attempts are required to analyze each factor in the future. Last, the accurate relationship between PM_{2.5} and total suspended particles should be investigated and accordingly considered in the proposed model.

IV. CONCLUSION

In this paper, we attempt to estimate the PM_{2.5} concentration by designing a photograph-based method. By observation, it is found that the saturation map is sensitive to air quality, exhibiting entirely different appearances under high and low PM_{2.5} concentrations. Specifically, it loses structures and most pixel values tend to be 0 under a high PM_{2.5} concentration. On this basis, we first compute the gradient similarity between the saturation and gray-scale maps to quantify the structural information loss. Then, utilizing the Weibull distribution to fit the saturation map, we are able to derive a value to estimate the color information. Finally, the PM_{2.5} concentration of an image can be estimated via the combination of the aforementioned two features followed by a nonlinear mapping procedure. Both numerical and visualized results on real captured data validate the effectiveness and superiority of the proposed method in comparison with the relevant state-of-the-art methods. In addition, the proposed method is very efficient.

ACKNOWLEDGMENT

The authors would like to thank the editors and the anonymous reviewers for their constructive comments, which greatly helped in improving this paper.

REFERENCES

- [1] C. A. Pope, III, *et al.*, “Lung cancer, cardiopulmonary mortality, and long-term exposure to fine particulate air pollution,” *J. Amer. Med. Assoc.*, vol. 287, no. 9, pp. 1132–1141, 2002.
- [2] K. Gu, J. Qiao, and W. Lin, “Recurrent air quality predictor based on meteorology- and pollution-related factors,” *IEEE Trans. Ind. Informat.*, vol. 14, no. 9, pp. 3946–3955, Sep. 2018.
- [3] G. Andria, G. Cavone, V. Di Lecce, and A. M. L. Lanzolla, “Model characterization in measurements of environmental pollutants via data correlation of sensor outputs,” *IEEE Trans. Instrum. Meas.*, vol. 54, no. 3, pp. 1061–1066, Jun. 2005.
- [4] Y. Chen, A. Ebenstein, M. Greenstone, and H. Li, “Evidence on the impact of sustained exposure to air pollution on life expectancy from China’s Huai River policy,” *Proc. Nat. Acad. Sci. USA*, vol. 110, no. 32, p. 12936–12941, 2013.
- [5] Y. Zhao, S. Wang, L. Duan, Y. Lei, P. Cao, and J. Hao, “Primary air pollutant emissions of coal-fired power plants in China: Current status and future prediction,” *Atmos. Environ.*, vol. 42, no. 36, pp. 8442–8452, 2008.
- [6] O. A. Postolache, J. M. D. Pereira, and P. M. B. S. Girao, “Smart sensors network for air quality monitoring applications,” *IEEE Trans. Instrum. Meas.*, vol. 58, no. 9, pp. 3253–3262, Sep. 2009.
- [7] F. A. Batzias and C. G. Siontorou, “Measuring uncertainty in lichen biomonitoring of atmospheric pollution: The case of SO₂,” *IEEE Trans. Instrum. Meas.*, vol. 58, no. 9, pp. 3207–3220, Sep. 2009.
- [8] Z. Geng, Q. Chen, Q. Xia, D. S. Kirschen, and C. Kang, “Environmental generation scheduling considering air pollution control technologies and weather effects,” *IEEE Trans. Power Syst.*, vol. 32, no. 1, pp. 127–136, Jan. 2017.
- [9] J. C. Chow, “Measurement methods to determine compliance with ambient air quality standards for suspended particles,” *J. Air Waste Manage. Assoc.*, vol. 45, no. 5, pp. 320–382, 1995.
- [10] C. Zhang *et al.*, “Hybrid measurement of air quality as a mobile service: An image based approach,” in *Proc. IEEE Int. Conf. Web Services (ICWS)*, Jun. 2017, pp. 853–856.
- [11] W. Malm, K. Kelley, J. Molenar, and T. Daniel, “Human perception of visual air quality,” *J. Air Pollution Control Assoc.*, vol. 30, no. 2, pp. 122–131, 1980.
- [12] G. Andria *et al.*, “Dosimetric characterization and image quality assessment in breast tomosynthesis,” *IEEE Trans. Instrum. Meas.*, vol. 66, no. 10, pp. 2535–2544, Oct. 2017.
- [13] G. Yue, C. Hou, T. Zhou, and X. Zhang, “Effective and efficient blind quality evaluator for contrast distorted images,” *IEEE Trans. Instrum. Meas.*, to be published, doi: [10.1109/TIM.2018.2868555](https://doi.org/10.1109/TIM.2018.2868555).
- [14] G. Yue, C. Hou, K. Gu, T. Zhou, and G. Zhai, “Combining local and global measures for DIBR-synthesized image quality evaluation,” *IEEE Trans. Image Process.*, vol. 28, no. 4, pp. 2075–2088, Apr. 2019.
- [15] G. Yue, C. Hou, K. Gu, S. Mao, and W. Zhang, “Biologically inspired blind quality assessment of tone-mapped images,” *IEEE Trans. Ind. Electron.*, vol. 65, no. 3, pp. 2525–2536, Mar. 2018.
- [16] A. De Angelis, A. Moschitta, F. Russo, and P. Carbone, “A vector approach for image quality assessment and some metrological considerations,” *IEEE Trans. Instrum. Meas.*, vol. 58, no. 1, pp. 14–25, Jan. 2009.
- [17] G. Yue, C. Hou, K. Gu, N. Ling, and B. Li, “Analysis of structural characteristics for quality assessment of multiply distorted images,” *IEEE Trans. Multimedia*, vol. 20, no. 10, pp. 2722–2732, Oct. 2018.
- [18] B. Li, G. Thomas, and D. Williams, “Detection of ice on power cables based on image texture features,” *IEEE Trans. Instrum. Meas.*, vol. 67, no. 3, pp. 497–504, Mar. 2018.
- [19] H. Sellahewa and S. A. Jassim, “Image-quality-based adaptive face recognition,” *IEEE Trans. Instrum. Meas.*, vol. 59, no. 4, pp. 805–813, Apr. 2010.
- [20] G. Yue, C. Hou, J. Lei, Y. Fang, and W. Lin, “Optimal region selection for stereoscopic video subtitle insertion,” *IEEE Trans. Circuits Syst. Video Technol.*, vol. 28, no. 11, pp. 3141–3153, Nov. 2018.
- [21] S. Shirmohammadi and A. Ferrero, “Camera as the instrument: The rising trend of vision based measurement,” *IEEE Instrum. Meas. Mag.*, vol. 17, no. 3, pp. 41–47, Jun. 2014.
- [22] H. Wang, X. Yuan, X. Wang, Y. Zhang, and Q. Dai, “Real-time air quality estimation based on color image processing,” in *Proc. IEEE Vis. Commun. Image Process. Conf.*, Dec. 2014, pp. 326–329.
- [23] Y. Li, J. Huang, and J. Luo, “Using user generated online photos to estimate and monitor air pollution in major cities,” in *Proc. 7th Int. Conf. Internet Multimedia Comput. Service*, 2015, p. 79.
- [24] C. Liu, F. Tsow, Y. Zou, and N. Tao, “Particle pollution estimation based on image analysis,” *PLoS ONE*, vol. 11, no. 2, p. e0145955, 2016.

- [25] Z. Pan, H. Yu, C. Miao, and C. Leung, "Crowdsensing air quality with camera-enabled mobile devices," in *Proc. 29th AAAI Conf. Innov. Appl.*, 2017, pp. 4728–4733.
- [26] E. Spyromitros-Xioufous *et al.*, "Towards improved air quality monitoring using publicly available sky images," in *Multimedia Tools and Applications for Environmental & Biodiversity Informatics*. Cham, Switzerland: Springer, 2018, pp. 67–92.
- [27] C. F. Bohren and D. R. Huffman, *Absorption and Scattering of Light by Small Particles*. Hoboken, NJ, USA: Wiley, 2008.
- [28] D. E. Abbey, B. E. Ostro, G. Fraser, T. Vancuren, and R. J. Burchette, "Estimating fine particulates less than 2.5 microns in aerodynamic diameter (PM_{2.5}) from airport visibility data in California," *J. Exposure Anal. Environ. Epidemiol.*, vol. 5, no. 2, pp. 161–180, 1995.
- [29] J.-L. Wang *et al.*, "Quantitative relationship between visibility and mass concentration of PM_{2.5} in Beijing," *J. Environ. Sci.*, vol. 18, no. 3, pp. 475–481, 2006.
- [30] G. Yue, C. Hou, and T. Zhou, "Blind quality assessment of tone-mapped images considering colorfulness, naturalness and structure," *IEEE Trans. Ind. Electron.*, to be published, doi: [10.1109/TIE.2018.2851984](https://doi.org/10.1109/TIE.2018.2851984).
- [31] K. Gu, J. Qiao, X. Min, G. Yue, W. Lin, and D. Thalmann, "Evaluating quality of screen content images via structural variation analysis," *IEEE Trans. Vis. Comput. Graphics*, vol. 24, no. 10, pp. 2689–2701, Oct. 2018.
- [32] J. Sun, Z. Xu, and H.-Y. Shum, "Image super-resolution using gradient profile prior," in *Proc. IEEE Conf. Comput. Vis. Pattern Recognit.*, Jun. 2008, pp. 1–8.
- [33] Z. Wang, E. P. Simoncelli, and A. C. Bovik, "Multiscale structural similarity for image quality assessment," in *Proc. 37th Asilomar Conf. Signals, Syst. Comput.*, vol. 2, Nov. 2003, pp. 1398–1402.
- [34] K. Gu *et al.*, "Saliency-guided quality assessment of screen content images," *IEEE Trans. Multimedia*, vol. 18, no. 6, pp. 1098–1110, Jun. 2016.
- [35] K. Gu, L. Li, H. Lu, X. Min, and W. Lin, "A fast reliable image quality predictor by fusing micro- and macro-structures," *IEEE Trans. Ind. Electron.*, vol. 64, no. 5, pp. 3903–3912, May 2017.
- [36] F. Scholz, "Inference for the weibull distribution," *Stat 498B Ind. Statist.*, vol. 632, pp. 6–10, 2008.
- [37] K. Gu, J. Qiao, and X. Li, "Highly efficient picture-based prediction of PM_{2.5} concentration," *IEEE Trans. Ind. Electron.*, vol. 66, no. 4, pp. 3176–3184, Apr. 2019, doi: [10.1109/TIE.2018.2840515](https://doi.org/10.1109/TIE.2018.2840515).
- [38] A. Mittal, R. Soundararajan, and A. C. Bovik, "Making a 'completely blind' image quality analyzer," *IEEE Signal Process. Lett.*, vol. 20, no. 3, pp. 209–212, Mar. 2013.
- [39] L. Zhang, L. Zhang, and A. C. Bovik, "A feature-enriched completely blind image quality evaluator," *IEEE Trans. Image Process.*, vol. 24, no. 8, pp. 2579–2591, Aug. 2015.
- [40] Q. Wu, Z. Wang, and H. Li, "A highly efficient method for blind image quality assessment," in *Proc. IEEE Int. Conf. Image Process. (ICIP)*, Sep. 2015, pp. 339–343.
- [41] K. Gu, W. Lin, G. Zhai, X. Yang, W. Zhang, and C. W. Chen, "No-reference quality metric of contrast-distorted images based on information maximization," *IEEE Trans. Cybern.*, vol. 47, no. 12, pp. 4559–4565, Dec. 2017.
- [42] P. V. Vu and D. M. Chandler, "A fast wavelet-based algorithm for global and local image sharpness estimation," *IEEE Signal Process. Lett.*, vol. 19, no. 7, pp. 423–426, Jul. 2012.
- [43] L. Li, W. Lin, X. Wang, G. Yang, K. Bahrami, and A. C. Kot, "No-reference image blur assessment based on discrete orthogonal moments," *IEEE Trans. Cybern.*, vol. 46, no. 1, pp. 39–50, Jan. 2016.
- [44] R. Ferzli and L. J. Karam, "A no-reference objective image sharpness metric based on the notion of just noticeable blur (JNB)," *IEEE Trans. Image Process.*, vol. 18, no. 4, pp. 717–728, Apr. 2009.
- [45] N. D. Narvekar and L. J. Karam, "A no-reference image blur metric based on the cumulative probability of blur detection (CPBD)," *IEEE Trans. Image Process.*, vol. 20, no. 9, pp. 2678–2683, Sep. 2011.
- [46] K. Bahrami and A. C. Kot, "A fast approach for no-reference image sharpness assessment based on maximum local variation," *IEEE Signal Process. Lett.*, vol. 21, no. 6, pp. 751–755, Jun. 2014.
- [47] K. Gu, D. Tao, J.-F. Qiao, and W. Lin, "Learning a no-reference quality assessment model of enhanced images with big data," *IEEE Trans. Neural Netw. Learn. Syst.*, vol. 29, no. 4, pp. 1301–1313, Apr. 2018.
- [48] E. P. Simoncelli and B. A. Olshausen, "Natural image statistics and neural representation," *Annu. Rev. Neurosci.*, vol. 24, no. 1, pp. 1193–1216, 2001.
- [49] K. He, J. Sun, and X. Tang, "Single image haze removal using dark channel prior," *IEEE Trans. Pattern Anal. Mach. Intell.*, vol. 33, no. 12, pp. 2341–2353, Dec. 2011.
- [50] H. Xu, J. Guo, Q. Liu, and L. Ye, "Fast image dehazing using improved dark channel prior," in *Proc. IEEE Int. Conf. Inf. Sci. Technol.*, Mar. 2012, pp. 663–667.



Guanghui Yue received the B.S. degree in communication engineering from Tianjin University, Tianjin, China, in 2014, where he is currently pursuing the Ph.D. degree in information and communication engineering with the School of Electrical and Information Engineering.

He joined the Beijing Key Laboratory of Computational Intelligence and Intelligent System, Faculty of Information Technology, Beijing University of Technology, Beijing, China, in 2017, for one month, as a Visiting Student. He has also been a joint Ph.D.

Student with the School of Computer Science and Engineering, Nanyang Technological University, Singapore, since 2017. His current research interests include bioelectrical signal processing, multimedia quality assessment, 3-D image visual discomfort prediction, and pattern recognition.



Ke Gu received the B.S. and Ph.D. degrees in electronic engineering from Shanghai Jiao Tong University, Shanghai, China, in 2009 and 2015, respectively.

He is currently a Professor with the Beijing University of Technology, Beijing, China. His current research interests include environmental perception, image processing, quality assessment, and machine learning.

Dr. Gu received the Best Paper Award from the IEEE TRANSACTIONS ON MULTIMEDIA, the Best

Student Paper Award at the IEEE International Conference on Multimedia and Expo in 2016, and the Excellent Ph.D. Thesis Award from the Chinese Institute of Electronics in 2016. He was the Leading Special Session Organizer in the VCIP 2016 and the ICIP 2017, and serves as a Guest Editor of the *Digital Signal Processing Journal*. He is currently an Associate Editor of the IEEE ACCESS and the *IET Image Processing*. He is a reviewer for 20 top SCI journals.



Junfei Qiao (M'11) received the B.E. and M.E. degrees in control engineering from Liaoning Technical University, Fuxin, China, in 1992 and 1995, respectively, and the Ph.D. degree from Northeastern University, Shenyang, China, in 1998.

He was a Post-Doctoral Fellow with the School of Automatics, Tianjin University, Tianjin, China, from 1998 to 2000. He joined the Beijing University of Technology, Beijing, China, where he is currently a Professor and also the Director of the Intelligence Systems Laboratory. His current research interests

include neural networks, intelligent systems, self-adaptive/learning systems, and process control systems.

Dr. Qiao is a member of the IEEE Computational Intelligence Society. He is a reviewer for more than 20 international journals, such as the IEEE TRANSACTIONS ON FUZZY SYSTEMS and the IEEE TRANSACTIONS ON NEURAL NETWORKS AND LEARNING SYSTEMS.